Droplets to Drops by Turbulent Coagulation

N. RIEMER*

Department of Mechanical and Aeronautical Engineering, University of California, Davis, Davis, California

A. S. WEXLER

Department of Mechanical and Aeronautical Engineering, Department of Civil and Environmental Engineering, and Department of Land, Air, and Water Resources, University of California, Davis, Davis, California

(Manuscript received 12 November 2003, in final form 30 September 2004)

ABSTRACT

This study addresses two central problems in cloud microphysics. The first is the source of large droplets, which initiates the rapid production of warm rain. The second is the broadening of the cloud droplet spectrum at both tails of the spectrum. The study explores how in-cloud turbulence can help to close the gaps in our understanding. With box model simulations, the development of cloud droplet spectra is calculated using a coagulation kernel that recently has been derived from direct numerical simulations. This kernel includes both the effect of turbulence on the relative velocities of the droplets and on the local increases in droplet concentration, the so-called accumulation effect. Under the assumption that this kernel can be extrapolated to atmospheric Reynolds numbers, the results show that for typical atmospheric conditions, the turbulent coagulation kernel is several orders of magnitude larger than the sedimentation kernel for droplets smaller then 100 μm. While for calm air after 30-min simulation time, only 7% of the total mass is found in droplets with sizes over 100 μm, this increases to 79% for a dissipation rate of 100 $\text{cm}^2\,\text{s}^{-3}$ and 96% for 300 $\text{cm}^2\,\text{s}^{-3}$ if a combined sedimentation and turbulent kernel is employed that assumes that the sedimentation and turbulent kernel can be added. Hence, moderate turbulence can enhance significantly the formation of large droplets. Furthermore, a time-scale analysis shows that broadening at the upper end of the spectrum is caused by turbulent coagulation whereas thermodynamic effects are responsible for broadening at the lower end.

1. Introduction

Rain formation and the role of clouds in climate and atmospheric chemistry are closely linked to evolution of the cloud-droplet spectra. As recent reviews state, our understanding of these processes is still fragmentary (Beard and Ochs 1993; Pinsky et al. 2000). The source of large droplets required to initiate the rapid production of warm rain in both maritime and continental clouds constitutes a major unknown in cloud physics. A related and also unexplained phenomenon is the observed broadening of the cloud-droplet spectrum with increasing height from cloud base at both the small and large ends of the spectrum (Warner 1969; Brenguier and Chaumat 2001). Various theories have been proposed to explain these observations, including mixing with the surroundings followed by fresh nucleation (Lee and Pruppacher 1977), collisions of large droplets arising from giant and ultragiant nuclei (Beard and Ochs 1993; Yin et al. 2000) and the self-broadening of the droplet spectrum by collision of cloud droplets due to the turbulence in clouds, which will be the topic of our investigation.

Arenberg (1939) realized that clouds are an inherently turbulent medium where turbulence could influence the droplet coagulation process, but this process is still not well understood and therefore insufficiently represented in current cloud models. In recent decades, several authors have revisited the area, some focusing on the industrial aspect of coagulating particles in a turbulent fluid (e.g., Kruis and Kusters 1997) and others on the atmosphere (e.g., Grover and Pruppacher 1985; de Almeida 1976).

Khain et al. (2000) and Shaw (2003) reviewed the state of the art of our understanding of particle–turbulence interactions in droplet-spectra evolution in clouds. They drew the conclusion that turbulence can enhance the collision kernel and hence the droplet growth significantly. More specifically, turbulence increases the geometric collision by three mechanisms. First, particle inertia leads to increased relative veloci-

* Current affiliation: Center for Turbulence Research, Stanford University, Stanford, California.

Corresponding author: A. S. Wexler, University of California, Davis, One Shields Avenue, Davis, CA 95616.
E-mail: aswexler@ucdavis.edu

ties and less-correlated velocity directions (acceleration effect). Second, the wind field shear produces collisions between particles even with the same inertia (shear effect; Saffman and Turner 1956). The acceleration and the shear effect are often referred to as the transport effect. Third, coagulation rates are enhanced because of local concentration increases for particle response times on the order of the Kolmorgorov scale. For this phenomenon the terms "preferential concentration" or "accumulation effect" have been coined. Depending on the relation between the governing time scales of the fluid and the particle response times, the impact of the transport and accumulation effects varies. The transport effect is most dominant if the particle response time τ_p is on the order of the flow integral time scale T_e, whereas the accumulation effect is most dominant if τ_p is on the order of the Kolmogorov time scale τ_k (Wang et al. 2000; Reade and Collins 2000).

Furthermore, turbulence can also alter the collision efficiency because of local aerodynamic droplet–droplet interactions. It should also be pointed out that turbulence may also influence condensational growth (e.g., Grabowski and Vaillancourt 1999; Shaw 2000; Vaillancourt et al. 2002), a process beyond the scope of this paper.

The most frequently cited study concerning the impact of turbulence on coagulation is certainly the pioneering work by Saffman and Turner (1956), which included the effect of turbulence on the relative velocity of the particles by the shear and accelerative mechanisms. However, as the authors clearly pointed out, it was restricted to low-inertia particles. Yet, considering the turbulence levels in the atmosphere and the size of cloud droplets, important inertial effects are expected.

In the mechanical engineering community, Abrahamson (1975) derived an approximation for the collision kernel for the large-particle limit treating the problem of dust separation in industrial cyclones. Williams and Crane (1983) combined Abrahamson's large-particle limit and Saffman and Turner's (1956) small-particle limit but only included the acceleration mechanism. Kruis and Kusters (1997) developed an improved formulation based on Williams and Crane (1983), which included the shear effect as well as the acceleration mechanism and was also reduced to the Saffman and Turner small-particle limit, which was not the case in the work of Williams and Crane (1983).

These aforementioned studies only treated the impact of turbulence on the relative velocity of droplets. Maxey (1987) first showed the phenomenon of preferential concentration, which was expanded by Squires and Eaton (1991) and Wang and Maxey (1993). Sundaram and Collins (1996) introduced the pair correlation function to quantify the effect of preferential concentration in the collision kernel. Since this work, further efforts have been made by Wang et al. (1998, 2000) and Zhou et al. (2001) to develop a model for the collision kernel on the basis of the solution of the Navier–Stokes equations using direct numerical simulations (DNS). While Kruis and Kusters (1997) did not include the accumulation effect, in these simulations both the transport and the accumulation effect were included.

A limitation of these studies with respect to their application to the atmosphere is certainly that they are carried out for nonsedimenting droplets. However, several authors (e.g., Pinsky and Khain 2001; Kostinski and Shaw 2001) measured the existence of small-scale concentration fluctuations in clouds, which strengthens the hypothesis that preferential concentration is also present in the atmosphere. Yet, our quantitative understanding of the interplay of turbulence and sedimentation is still poor and further efforts have to be undertaken to improve this situation.

Direct numerical simulations are furthermore limited by the modest range of Reynolds numbers that can be covered. Wang et al. (2000) argued that the accumulation effect becomes even more pronounced for high Reynolds number flow, which is typical for atmospheric conditions, but further work has to be done to support or reject this hypothesis.

While most of the studies mentioned above focused on engineering flows, Pinsky and Khain (1997a) addressed the cloud physics community. In a series of studies these authors explored the impact of turbulence on the collision of atmospheric droplets, starting from a simple shear flow (Khain and Pinsky 1995) to a model of Batchelor turbulence (Pinsky and Khain 1996, 1997a,b; Khain and Pinsky 1997). To represent the accumulation effect, Pinsky and Khain (1997a) added a term proportional to the rms drop-velocity flux divergence in the stochastic coalescence equation.

Finally, Pinsky et al. (1999) investigated the impact of turbulence on the collision efficiency. The authors concluded that in turbulent flows the collision efficiency can be significantly enhanced compared to that in calm air.

Experimental studies are rare compared to the theoretical ones, especially in the parameter range that relates to atmospheric clouds. Obviously, it is impossible to cover the entire turbulent kinetic energy spectrum present in natural clouds with laboratory experiments. Woods et al. (1972), Jonas and Goldsmith (1972), and Neizvestny and Kobzunenko (1986) all conclude from their experiments that turbulence enhances drop collision, however, their experiments were limited to relatively small collector drops. Vohl et al. (1999) confirmed for larger collector drops that the droplets grow faster in turbulent flow compared to laminar flow.

As can be seen from the brief literature review above, many of the theoretical studies have been devoted to the derivation of collision kernels. Few studies, however, investigate the resulting development of droplet size distributions (Park et al. 2002; Pinsky and Khain 1997c). In light of the recent DNS-derived kernels we explore the possible impact of turbulence on the droplet size distribution for atmospheric conditions systematically, and address two questions, namely:

Does turbulence have the potential to enhance the coagulation process sufficiently to rapidly form large droplets and explain the observed production of warm rain?

Can our predictions work toward reproducing the observed broadening of the size distribution?

We will simulate the evolution of the droplet size distribution using the coagulation kernel presented by Zhou et al. (2001), since their parameterization covers the accumulation and the transport effects. By applying this parameterization to atmospheric conditions, the potential influence of turbulent coagulation is evaluated.

It should be pointed out that investigations of turbulence on cloud microphysics are recently undergoing a very fast development and the analysis of various important aspects of this topic has just started. Therefore, this study should be understood as a first approach to incorporate DNS results in atmospheric models, being aware of the simplification that had to be made at this stage. In particular, the limitations of our study consist of the following underlying assumptions: First, the DNS simulations that are the basis for the turbulent coagulation kernel we used did not include gravitational effects. Second, the DNS simulations were performed at a much lower Reynolds number than those present in the atmosphere. The implications of both assumptions are discussed later in this paper.

In the following section, the calculation of the turbulent collision kernel is outlined along with an overview of the parameter values that are the basis for those calculations. Section 3 presents numerical results of a box model simulating the development of cloud-droplet spectra using the turbulent kernel for different atmospheric conditions. Furthermore, the concept of timescale analysis is introduced comparing the time scale for condensation and coagulation for atmospheric conditions. Finally, concluding remarks are given in section 4.

2. Method

a. The collision kernel

Zhou et al. (2001) provide a model to predict the geometric collision kernel in a bidisperse system for a turbulent fluid, which is derived from direct numerical simulations. This model includes both the turbulent transport effect and the accumulation effect. In our work, we apply this kernel to calculate the development of cloud-droplet spectra under atmospheric conditions. The following section outlines the calculation of the collision kernel in a turbulent fluid.

The ensemble average of the collision kernel $K_t(r_1, r_2)$ for two particles with the radii r_1 and r_2 in a turbulent fluid can be expressed in a generalized form by (Sundaram and Collins 1997):

$$K_t(r_1, r_2) = E_t \Gamma_0 \frac{\langle |w_r(r_1, r_2)| \rangle}{\langle |w_{r,\text{shear}}(r_1, r_2)| \rangle} g_{12}(R), \qquad (1)$$

where $R = r_1 + r_2$ is the collision radius and

$$\Gamma_0 = \sqrt{\frac{8\pi}{15}} R^3 \frac{\upsilon_k}{\eta}$$

is the collision kernel for zero-inertia particles according to Saffman and Turner (1956), with the Kolmogorov velocity scale $\upsilon_k = (\nu\epsilon)^{1/4}$, where ν is the viscosity of the fluid and ϵ the dissipation rate. The Kolmogorov length scale is $\eta = (\nu^3/\epsilon)^{1/4}$ and E_t is the turbulent collection efficiency.

The collection efficiency is E_t defined as the product of the collision efficiency $E_{\text{col},t}$ and the coalescence efficiency $E_{\text{coa},t}$. The collision efficiency represents the ratio of the actual number of collisions to the number for complete geometric sweep-out. However, collision does not guarantee coalescence. The coalescence efficiency accounts for this fact and is defined as the ratio of the number of coalescences to the number of collisions.

The hydrodynamic interactions of droplets in turbulent flow are highly uncertain, but there are indications that $E_{\text{col},t}$ is larger in turbulence than in calm air (Pinsky et al. 1999). In our study we retain the value $E_{\text{col},t} = 1$, and we give an estimation of the impact of $E_{\text{col},t}$ based on the work of Pinsky et al. (1999) in the appendix. Even less is known about $E_{\text{coa},t}$, the coalescence efficiency in turbulent flow. Laboratory studies of small colliding droplets show that the coalescence efficiency is close to 1 if the droplets are charged and an electrical field is present (Rogers and Yau 1989). Because weak fields and charges exist in natural clouds, we therefore assume $E_{\text{coa},t} = 1$ for the sake of simplicity.

The term $\langle |w_r(r_1, r_2)| \rangle / \langle |w_{r,\text{shear}}(r_1, r_2)| \rangle$ with its two components—shear and acceleration—represent the turbulent transport effect by

$$\langle |w_{r,\text{shear}}(r_1, r_2)| \rangle = \sqrt{\frac{2}{15\pi}} \upsilon_k \frac{R}{\eta}, \frac{\langle |w_r(r_1, r_2)| \rangle}{\langle |w_{r,\text{shear}}(r_1, r_2)| \rangle} = \left[1 + 15 \frac{w_{r,\text{accel}}^2}{\upsilon_k^2} \left(\frac{\eta}{R} \right)^2 \right]^{1/2}$$

$$\frac{w_{r,\text{accel}}^2}{\upsilon_k^2} = C_w(\phi) \left(\frac{u'}{\upsilon_k} \right)^2 \frac{\gamma}{\gamma - 1} \left[(\theta_1 + \theta_2) - \frac{4\theta_1\theta_2}{(\theta_1 + \theta_2)} \sqrt{\frac{1 + \theta_1 + \theta_2}{(1 + \theta_1)(1 + \theta_2)}} \right]$$

$$\times \left[\frac{1}{(1 + \theta_1)(1 + \theta_2)} - \frac{1}{(1 + \gamma\theta_1)(1 + \gamma\theta_2)} \right], \qquad (2)$$

where $\theta_i = 2.5\ \tau_p(r_i)/T_e$ ($i = 1, 2$) is proportional to the ratio of particle response time $\tau_p = 2\rho_p r_i^2/(9\nu\rho)$ to flow integral time $T_e = u'^2/\epsilon$. Here, ρ_p is the particle density, ρ the fluid density, r_i particle radius, and u' the fluid rms velocity fluctuation.

Equation (2) is developed on the basis of the formulation by Kruis and Kusters (1997). To fit their numerical results, Zhou et al. (2001) introduced the function $C_w(\phi) = 1.0 + 0.6\exp[-(\phi - 1)^{1.5}]$ and the factor $\gamma = \phi \times 0.183u'^2/\sqrt{\epsilon\nu}$ with $\phi = \max(\theta_2/\theta_1, \theta_1/\theta_2)$.

The factor

$$g_{12}(R) = 1 + \rho_{12}\sqrt{g_{11}(R) - 1}\sqrt{g_{22}(R) - 1}$$

is the bidisperse radial distribution function at contact and accounts for the accumulation effect, which is governed by the monodisperse radial distribution functions g_{ii} (i = 1, 2; no summation implied) and the concentration correlation coefficient

$$\rho_{12} = 2.6\exp(-\psi) + 0.205\exp(-0.0206\psi) \times \frac{1}{2}[1 + \tanh(\psi - 3)],$$

where $\psi = \max(\tau_{p2}/\tau_{p1}, \tau_{p1}/\tau_{p2})$ and

$$g_{ii} = 1 + y_0(\alpha)[1 - z_0^2(\alpha)] + R_\lambda z_0^2(\alpha)\{y_1(\alpha)[1 - z_1(\alpha)] + y_2(\alpha)z_1(\alpha) + y_3(\alpha)z_2(\alpha)\}. \quad (3)$$

The functions $y_0(\alpha)$, $y_1(\alpha)$, $y_2(\alpha)$, $y_3(\alpha)$, $z_0(\alpha)$, $z_1(\alpha)$, and $z_2(\alpha)$ are given in Table 1. Here, the argument $\alpha = \tau_{pi}/\tau_k$ is the Stokes number where $\tau_k = \sqrt{\nu/\epsilon}$ is the Kolmogorov time scale.

The monodisperse radial distribution function g_{ii} scales with the Taylor microscale Reynolds number, which is defined as $R_\lambda = u'\lambda/\nu$ with the transverse Taylor microscale $\lambda = \sqrt{15\nu u'^2/\epsilon}$. The linear dependence of g_{ii} on R_λ is based on the results of direct numerical simulations, which only cover a range of low Reynolds numbers compared to atmospheric conditions. The extrapolation of this relationship to high Reynolds numbers introduces therefore some uncertainty, which we must keep in mind when interpreting our results.

Furthermore, Zhou et al. (2001) employ the following assumptions in their model: The size of the particles is on the order of or less than the Kolmogorov length scale η. The particle volume fraction and mass loading are sufficiently low so that the presence of the particles does not impact the gas turbulence. These assumptions are valid for clouds as established in section 2.2.

Moreover, their DNS simulations do not include the effect of gravity. In the atmosphere, both turbulence and gravitation clearly affect the size distribution and therefore it is necessary to formulate a collision kernel that includes both mechanisms. The usual approach for modeling the impact of several coagulation mechanisms such as Brownian motion and gravitational settling is simply to add the individual kernels. As Butuirat and Kielkiewicz (1996) show, this method gives satisfying results. They investigate two cases, namely Brownian and turbulent shear coagulation, and Brownian, gravitational, and turbulent shear coagulation. However if the accumulation effect is also involved, the formulation of the resulting kernel requires more caution. Vaillancourt and Yau (2000) discuss the relative roles of sedimentation and turbulence. An appropriate nondimensional diameter (S_υ) is the ratio of the eddy turnover time to the time it takes for the particles to sediment across the eddy, which we can also express as the ratio of the settling velocity of the particles υ_T and the Kolmogorov velocity scale υ_k: $S_\upsilon = \upsilon_T/\upsilon_k$. If $S_\upsilon \ll 1$ sedimentation is negligible, if $S_\upsilon \gg 1$ the particles will quickly sediment through the eddy which decreases the particle–eddy interaction. For droplets of interest in the atmosphere, S_υ is usually larger than 1, which means that the impact of gravitational settling might weaken the impact of the accumulation effect. Indeed Wang and Maxey (1993) have shown that for Stokes numbers of 1, preferential concentration decreases slightly as S_υ increases from 0 to 3. On the other hand, Wang and Maxey (1993) also show that the mean settling velocity for particles with Stokes numbers around 1 increases in a turbulent flow compared to calm air. The overall effect of the interaction of gravitation and turbulence on the coagulation of particles is still not very well understood at this stage and represents an area where further research is needed.

If not otherwise indicated, we will consider the effect of gravity and turbulence separately. To estimate the interaction of these processes, we simply add the turbulent and sedimentation kernels. This approach is clearly only preliminary and will be improved as research progresses.

In our investigation the sedimentation kernel $K_s(r_1, r_2)$ for calm air will be employed for comparison, which is given by

$$K_s(r_1, r_2) = \pi(r_1 + r_2)^2 E_s|\upsilon_T(r_1) - \upsilon_T(r_2)|. \quad (4)$$

Here, E_s is the collision efficiency for calm air where we use the values provided by Hall (1980), and $\upsilon_T(r_1)$,

TABLE 1. Auxiliary functions for the radial distribution function g_{ii}.

$$y_0(\alpha) = 18\ \alpha^2$$
$$y_1(\alpha) = 0.36\alpha^{2.5}\exp(-\alpha^{2.5})$$
$$y_2(\alpha) = 0.24\exp(-0.5\ \alpha)$$
$$y_3(\alpha) = 0.013\exp(-0.07\ \alpha)$$
$$z_0(\alpha) = \frac{1}{2}\left(1 + \tanh\frac{\alpha - 0.5}{0.25}\right)$$
$$z_1(\alpha) = \frac{1}{2}\left(1 + \tanh\frac{\alpha - 1.25}{0.1}\right)$$
$$z_2(\alpha) = \frac{1}{2}\left(1 + \tanh\frac{\alpha - 6.5}{2.5}\right)$$

$v_T(r_2)$ are the terminal velocities of the droplets in calm air.

b. Calculation of the size distributions

The stochastic collection equation describes the evolution of a colliding and coalescing cloud droplet size distribution (Pruppacher and Klett 1997);

$$\frac{\partial n(m,t)}{\partial t} = \frac{1}{2}\int_{m_0}^{m} n(m_c,t)K(m_c,m')n(m',t)dm' - \int_{m_0}^{\infty} n(m,t)K(m,m')n(m',t)dm',$$

where $n(m, t)$ is the drop number distribution function at time t and $K(m_c, m')$ is the collection kernel describing the rate at which a droplet of mass $m_c = m - m'$ is collected by a droplet of mass m' forming a droplet of mass m. The following transformation of variables leads to the stochastic collection equation for the mass size distribution $g(y, t)$ (Berry 1967):

$$g(y,t)dy = mn(m,t)dm, \quad n(m,t) = \frac{1}{3m^2}g(y,t),$$

where $y = \ln r$ and r is the radius of droplets with mass m; and

$$\frac{\partial g(y,t)}{\partial t} = \frac{1}{2}\int_{y_0}^{y} \frac{m^2}{m_c^2 m'} g(y_c,t)K(y_c,y')g(y',t)dy' - \int_{y_0}^{\infty} g(y,t)\frac{K(y,y')}{m'}g(y',t)dy'. \quad (5)$$

As an initial cloud droplet distribution we use a Gamma function of the form $n(m, t = 0) = L_w/\overline{m}^2 \exp(-m/\overline{m})$, where L_w is the total cloud water content and $\overline{m}$ is the mean droplet mass. Assuming spherical droplets, $\overline{m}$ and the mean droplet radius $\bar{r}$, are related by $\overline{m}(r) = 4/3\pi\rho_p\bar{r}^3$, where ρ_p is the water density.

For our simulations, L_w is set to 1 g m^{-3}, typical for warm rain clouds and $\bar{r}$ to 10 μm, a typical cloud droplet size. This means that the assumptions mentioned above (low mass loading and particles smaller than or on the order of η) hold. The solution of the stochastic collection Eq. (5) uses the flux method by Bott (1998), which has been proved to be both efficient and mass conservative. For the collection kernel K we employ the turbulent collision kernel K_t as described in section 2.1 for different atmospheric conditions, and compare the results to those obtained with the kernel for sedimentation in calm air K_s [Eq. (4)].

Cloud dissipation rates ϵ depend on cloud type and age. The values range from 10 cm^2 s^{-3} for stratus clouds to several 100 cm^2 s^{-3} for cumuli and 1000 cm^2 s^{-3} for cumulonimbus clouds (Pruppacher and Klett 1997).

Figure 1 shows measured dissipation rates ϵ in clouds with the corresponding rms velocity u' (MacPherson and Isaac 1977). From dimensional arguments, a cubic relation between ϵ and u' is expected, since

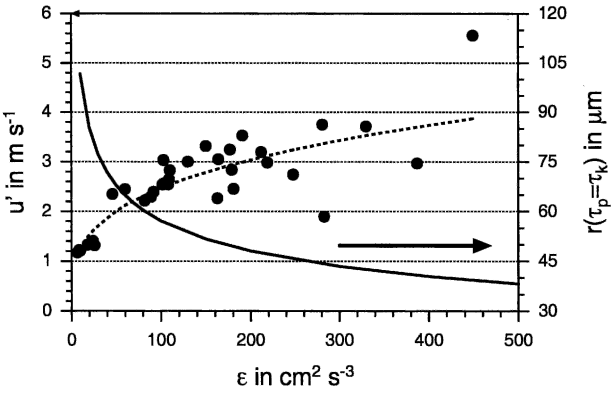

FIG. 1. Measured values of u' and ϵ in clouds (dots; MacPherson and Isaac 1977). Broken line is the fit of measured data; solid line is particle radius for which $\tau_p = \tau_k$.

$$\epsilon = \frac{u'^3}{L}, \quad (6)$$

as long as the characteristic length scale L is relatively constant. The broken line shows the fit to the data points for $L = 1500$ m. The solid line shows the radius r_k that fulfills the condition $\tau_p(r_k) = \tau_k(\epsilon)$, showing that the accumulation effect is important.

For values of ϵ that occur in the atmosphere, the values for r_k are in the range of observed cloud droplet sizes. Therefore, the accumulation effect is expected to be significant for droplets between 30 and 100 μm. The transport effect, however, is less important since $\tau_p = T_e$ applies for unreasonably large particle sizes under atmospheric conditions.

In the following, the values of $\epsilon = 300$ cm^2 s^{-3} and $u' = 3.5$ m s^{-1} are used for the base case, which fulfill Eq. (6) and represent in-cloud turbulence of moderate to high intensity.

3. Results and discussion

In this section we investigate various aspects of the influence of turbulence on the development of the droplet size distribution. First, we compare the magnitude of the coagulation kernel due to sedimentation to the turbulent coagulation kernel according to Zhou et al. (2001) for atmospheric conditions. Then we evaluate the influence of different turbulence levels on the evolution of the drop size spectra. Furthermore, we will introduce the concept of a time-scale analysis, which will help us to interpret the results and to compare the processes of coagulation and condensation with respect to their ability to broaden the size distribution.

Figure 2 shows the turbulent coagulation kernel K_t according to Eq. (1) for the base case, and Fig. 3 shows

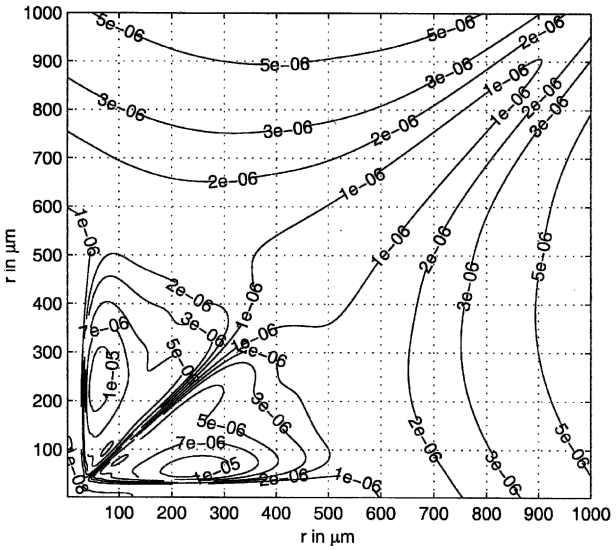

FIG. 2. Turbulent coagulation kernel K_t in $m^3 s^{-1}$ for $\epsilon = 300$ $cm^2 s^{-3}$ and $u' = 3.5$ m s^{-1}.

the relative differences $(K_t - K_s)/K_s$ to the sedimentation kernel K_s according to Eq. (4). Given Eq. (4), it is clear that K_s becomes large if the sizes of the colliding droplets are different and zero for equally sized droplets. The turbulent coagulation kernel K_t exhibits a distinct local maximum for the combination of droplet radii near 65 and 250 μm using the base case values for ϵ and u'. The exact position, as well as the magnitude of this maximum, depends on ϵ and u'. Note that this local maximum in the 65- to 250-μm size range is not of primary importance for the onset of effective coagulation. To be effective, turbulent coagulation must help particle grow through the 10- to 40-μm gap; condensation grows particles below this size and settling coagulation grows particles above it. Figure 3 shows that the turbulent coagulation kernel is much larger than settling in this size range and is also effective for particles of similar size. We can therefore expect that the impact of turbulent coagulation is especially significant in the initial stage of the development of the cloud whereas the impact decreases for large cloud droplets or raindrops. Figure 4 shows what combination of radii produces a local maximum in the turbulent kernel. The numbers in the figure denote the respective dissipation rate ϵ in $cm^2 s^{-3}$. The maximum shifts to larger radii for smaller dissipation rates, which means that higher dissipation rates enhance the coagulation process at an earlier stage.

Figures 5 and 6 show the development of the mass distribution $g(\ln r)$ with time for the sedimentation kernel and for the turbulent kernel for the base case. The top figures show as an overview the evolution for the full simulation period of one hour. Since the first 20 to 30 min is the crucial period for large droplet production, the bottom figures in Figs. 5 and 6 display the evolution during the first 30 min in more detail.

For the sedimentation kernel a second mode appears only after about 30 min. At $t = 30$ min, most of the mass (97%) is still distributed over the droplet size range smaller than 100 μm, confirming the well-known fact that sedimentation alone cannot explain the fast formation of large droplets. For the turbulent kernel, the second mode forms already after 10 min, because the turbulent coagulation kernel of Zhou et al. (2001) accelerates the formation of large drops. For simulation

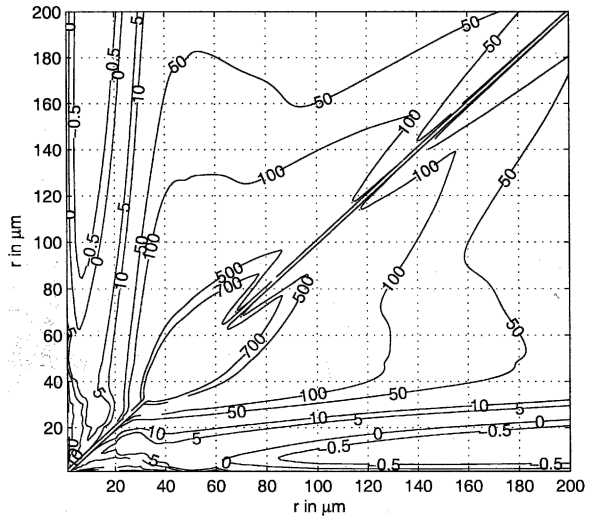

FIG. 3. Relative differences $(K_t - K_s)/K_s$; K_t as in Fig. 2. Note the different scale of the axis.

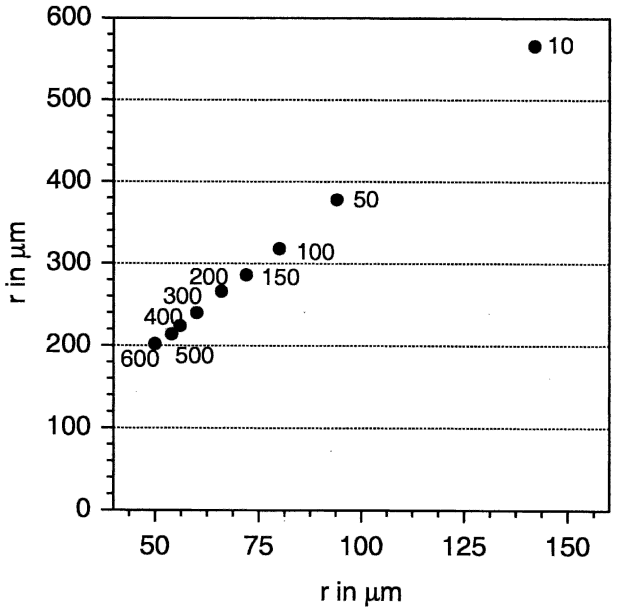

FIG. 4. Combination of radii for which the maximum of the coagulation kernel occurs for a given dissipation rate. The numbers denote the respective dissipation rate in $cm^2 s^{-3}$.

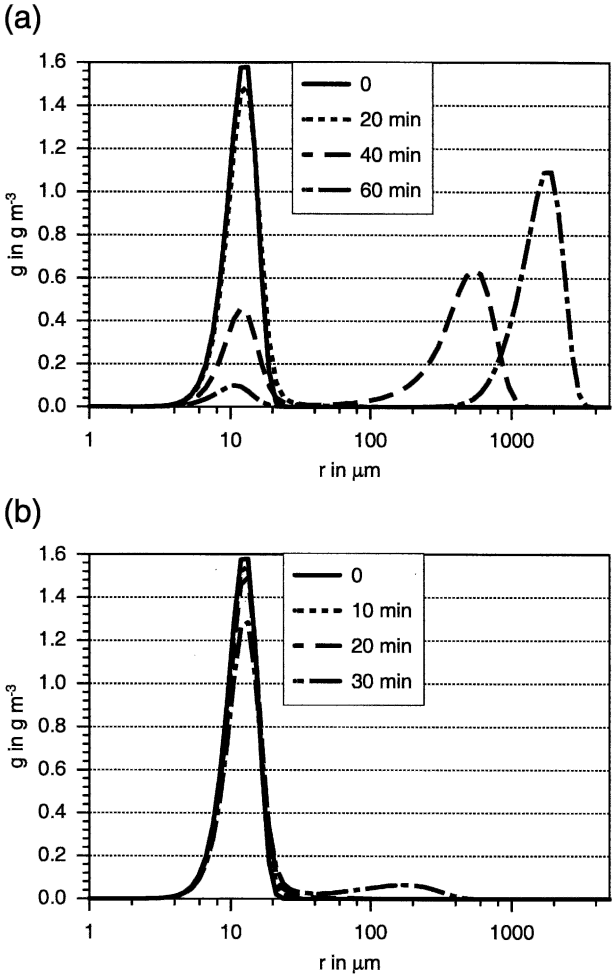

FIG. 5. (a) Temporal evolution of the mass size distribution with sedimentation kernel according to Hall (1980). (b) Evolution for the first 30 min in more detail.

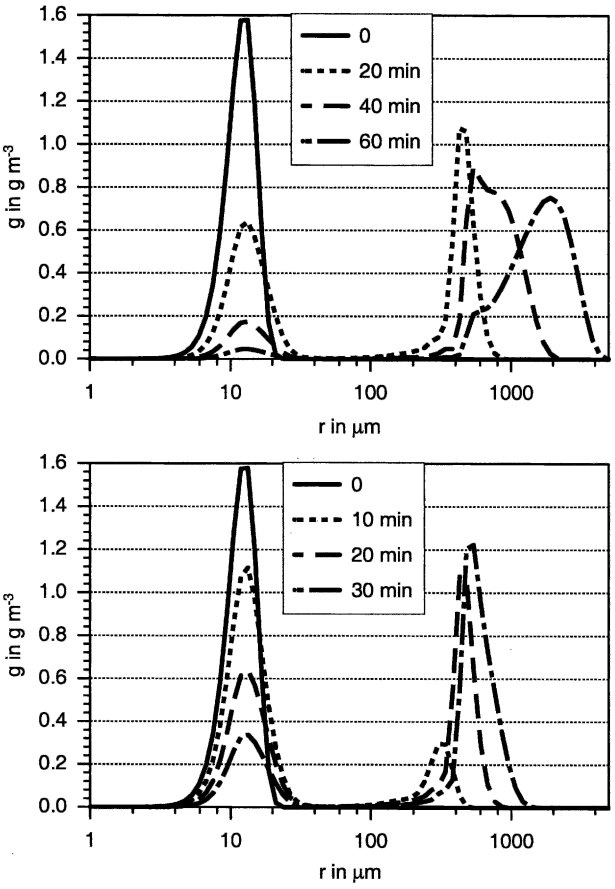

FIG. 6. Same as Fig. 5 but for the turbulent kernel, base case.

times around one hour, the sedimentation and turbulent kernels predict similar distributions, supporting the finding that turbulence is especially important for the early stage of the development of the cloud. Figure 7 shows the effect of the combined sedimentation and turbulent kernel. For this case, the second mode becomes visible after only 5 min, and after 30 min, 96% of the mass is transferred to sizes larger than 100 μm.

The sensitivity of the temporal evolution of the size distribution to ϵ is displayed in Fig. 8. It shows the development of the mass distribution $g(\ln r)$ for $\epsilon = 100$ cm^2 s^{-3}, $\epsilon = 200$ cm^2 s^{-3}, $\epsilon = 300$ cm^2 s^{-3}, and $\epsilon = 400$ cm^2 s^{-3} with the corresponding u' values according to Eq. (6). It is obvious that higher dissipation rates cause faster formation of large droplets. While for $\epsilon = 100$ cm^2 s^{-3}, the second mode appears after 25 min (comparable to sedimentation only), for $\epsilon = 400$ cm^2 s^{-3}, it appears only after 5 min.

As mentioned above, some uncertainty is introduced in the calculation of the coagulation kernel since we assume that the radial distribution function g_{12} depends linearly on the Reynolds number. While this assumption holds for the range of Reynolds numbers that are covered in direct numerical simulations, it is unknown if this will be still the case for Reynolds numbers in the

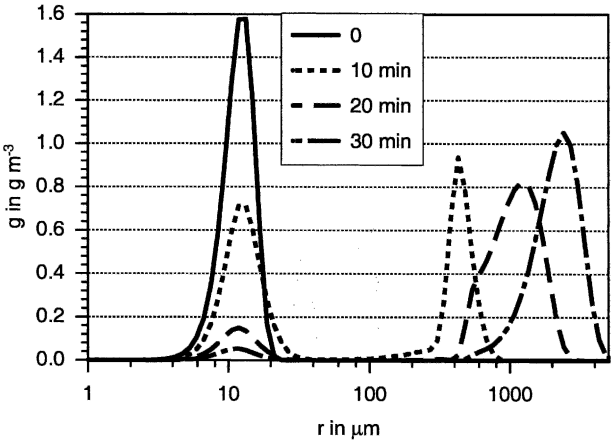

FIG. 7. Same as Fig. 5 but for the combined sedimentation and turbulent kernel.

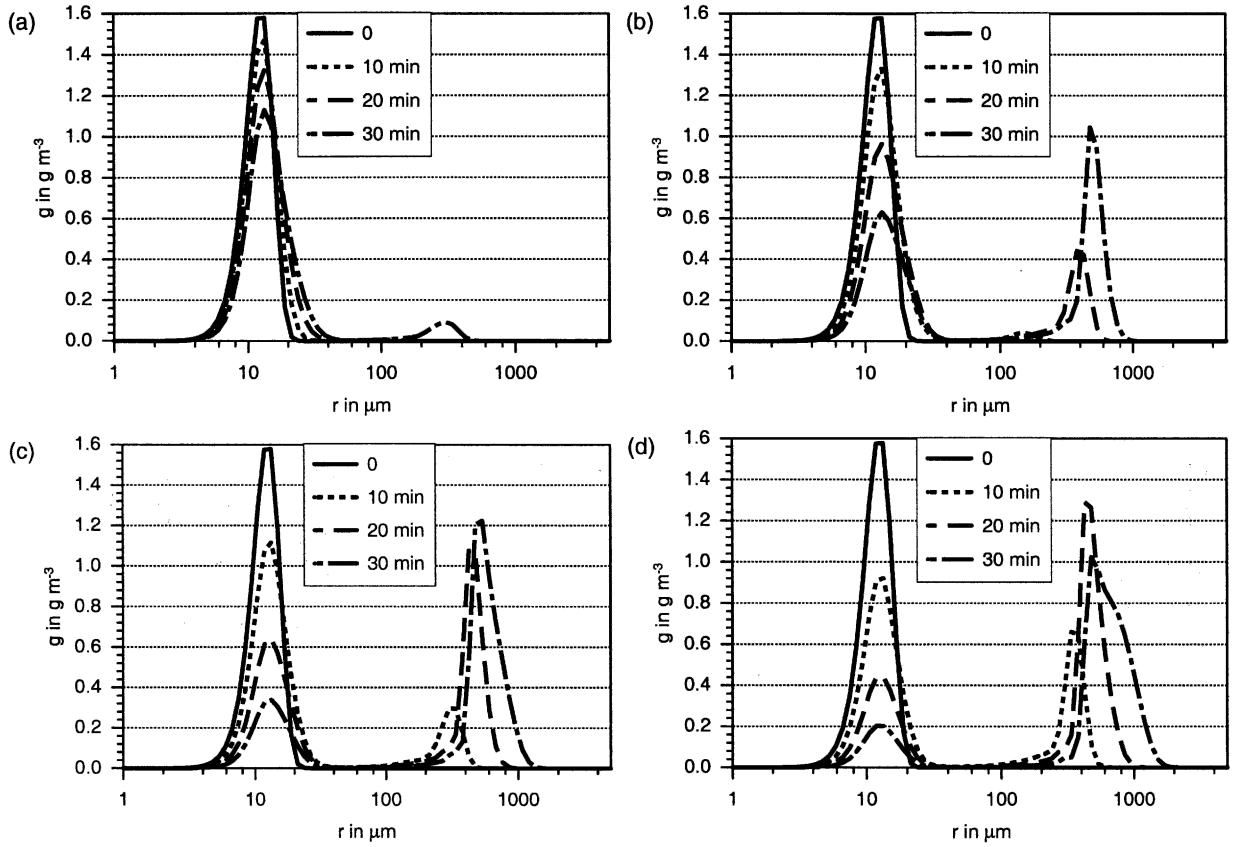

FIG. 8. Temporal evolution of the mass size distribution with turbulent kernel (a) $\epsilon = 100$ cm^2 s^{-3}, $u' = 2.5$, (b) $\epsilon = 200$ cm^2 s^{-3}, $u' = 3.0$ m s^{-1}, (c) $\epsilon = 300$ cm^2 s^{-3}, $u' = 3.5$ m s^{-1}, and (d) $\epsilon = 400$ cm^2 s^{-3}, $u' = 3.7$ m s^{-1}.

atmosphere or if g_{12} will level off after some (likewise unknown) threshold value is reached. Such behavior has been found for other problems in turbulence. For instance, Belin et al. (1997) show for the velocity gradient distributions in turbulence that a change in the dependence of the parameters of the distributions on the Reynolds number can be found around $R_\lambda = 700$. To estimate the sensitivity in our model we carry out an additional simulation where R_λ in Eq. (3) is set artificially to 700 while ϵ and u' are set to the base case values. Moreover, the combined sedimentation and turbulent kernel is employed. The result in Fig. 9 shows that compared to Fig. 7, the development of large droplets is clearly delayed. However, compared to Fig. 5 (sedimentation only), a strong acceleration of the large droplet formation within the first 30 min can still be noticed.

Time-scale analysis

In all cases, a characteristic gap between the initial mode and the developing second mode is apparent. This gap becomes narrower for larger ϵ, hence the dissipation rate controls the position of the second mode. Gaps in a size distribution imply that droplet lifetimes are so short that the droplets leave this size range very quickly. Here we develop a time-scale analysis to characterize the relevant processes and help to interpret the results. This analysis will also be used to address the problem of the size distribution broadening, a feature observed for both tails of cloud droplet size distribu-

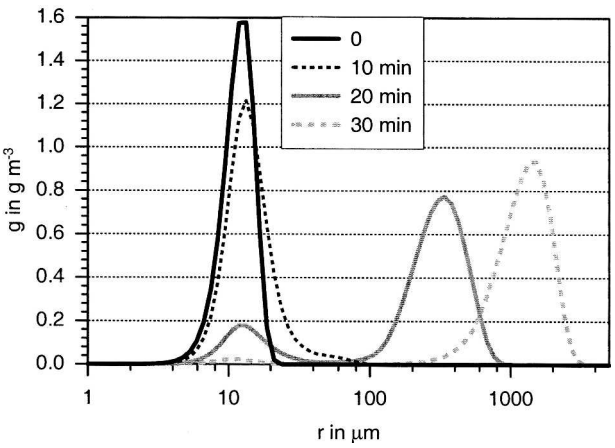

FIG. 9. Same as Fig. 7, but R_λ in Eq. (3) set to 700.

tions as the air parcel is ascending and cooling. Although this finding could partially be attributed to measurement artifacts, measured distributions at the cloud base are still found, in fact, to be narrower than distributions at higher elevation (Brenguier and Chaumat 2001).

Condensation and coagulation are both shaping the droplet size distribution and can cause a narrowing or broadening of the spectrum. While condensation typically dominates the droplet growth when the droplets are still small, coagulation becomes more important as larger droplets form. The time scales indicate which processes are faster, hence more important, for a given size and time under given conditions. We will use this analysis to compare the growth time scales due to condensation and turbulent coagulation.

The time scale $\tau(r)$ for the growth of a spherical particle of mass $m(r)$ and radius r is generally given by (Friedlander 1977; Kerminen and Wexler 1995):

$$\frac{1}{\tau(r)} = \frac{1}{r}\frac{dr}{dt} = \frac{1}{3m(r)}\frac{dm(r)}{dt}.$$

Broadening at the right tail of the distribution generally implies that $\tau(r)$ is decreasing with increasing r, meaning that larger droplets grow faster than smaller ones. Broadening at the left tail of the distribution cannot be achieved by coagulation. It requires a droplet evaporation or the formation of new droplets. For the latter, entrainment processes are thought to be responsible (Lee and Pruppacher 1977). For evaporation, thermodynamic processes, such as the trading of water between droplets of different sizes, are a possible mechanism (Majeed and Wexler 2001). In the following, the time scales for condensation and coagulation are specified.

1) CONDENSATION

The time scale τ_{cond} is defined as (Majeed and Wexler 2001)

$$\frac{1}{\tau_{\text{cond}}(r)} = \frac{1}{3m(r)}\frac{dm(r)}{dt} = \frac{1}{3m(r)} \times \frac{4\pi r D_v' M_w p^\circ(T_\infty)/(RT_\infty)[\text{RH} - \exp(A - B)]}{1 + [4\pi r D_v' M_w p^\circ(T_\infty)/(RT_\infty)][\Delta H_v M_w/(RT_\infty)][\Delta H_v/(4\pi r k_a' T_\infty)]\exp(A - B)}, \quad (7)$$

with

$$A = \frac{2M_w\sigma_w}{RT_a\rho_w r},$$

$$B = \nu_m \frac{M_w}{M_s}\frac{m_s}{m_d - m_p},$$

where M_w is the molecular weight of water vapor, M_s the molecular weight of the solute, R the universal gas constant, D_v' the water diffusivity corrected for noncontinuum effects, T_∞ the temperature of the environment, T_a the droplet temperature, $p^\circ(T_\infty)$ the water saturation pressure at T_∞, RH the relative humidity, ΔH_v the latent heat of water, k_a' the thermal conductivity corrected for noncontinuum effects, σ_w the air–water surface tension, ρ_w the water density, ν_m the number of ions per solute molecule, and m_s, m_d, and m_p the masses of solute, droplet, and dry particle, respectively.

In their study, Majeed and Wexler (2001) consider an ascending air parcel and show that the Kelvin effect leads to a characteristic trading of water between the small and the large droplets.

For our purpose, a state of equilibrium is considered: The relative humidity is calculated so that the droplets with the radius of the transport mean, $\bar{r}$, have zero growth: $dm(\bar{r})/dt = 0$. The other initial conditions are $T_\infty = 276$ K, $\nu_m = 3$, $M_s = 142$ g mole^{-1}, and $m_s = 10^{-19}$ kg.

Droplets with a radius smaller than $\bar{r}$ are evaporating because of the Kelvin effect, droplets with a larger radius are growing (however, very slowly). Equally sized droplets grow or evaporate all with the same rate.

2) COAGULATION

The crucial difference between growth by condensation and coagulation is that coagulation causes particles of the same size to grow at different rates. Depending on the partner they coagulate with, droplets in a bin of size i will end up in different bins after one time step. Nevertheless a similar time scale for the growth can be defined, however note that this is an averaged expression for the growth of one particle of size r.

Given the size distribution $n(r)$, where the total number density N is given by $N = \int_0^\infty n(r)\mathrm{d}r$, and the mass distribution $g(r)$, where $g(r) = m(r)n(r)$. The time scale τ_{coag} is then defined as

$$\frac{1}{\tau_{\text{coag}}(r)} = \frac{1}{3n(r)m(r)}\int_0^\infty n(r)K(r, r')n(r')m(r')\mathrm{d}r' = \frac{1}{3m(r)}\int_0^\infty g(r')K(r, r')\mathrm{d}r'. \quad (8)$$

The numerator represents the increase in mass of the droplets with radius r due to the coagulation with any other droplets. Dividing by $n(r)$ and normalizing by $3m(r)$, this gives the growth rate per droplet and therefore compares to $\tau_{\text{cond}}(r)$.

To help understand the effects of coagulation on growth, we define the time scales $\tau_{\text{coag}}^-(r)$ and $\tau_{\text{coag}}^+(r)$ by modifying the limits of the integral in Eq. (8). The time scale $\tau_{\text{coag}}^+(r)$ represents the growth due to larger droplets and $\tau_{\text{coag}}^-(r)$ represents the growth due to smaller droplets:

$$\frac{1}{\tau^{-}_{\text{coag}}(r)} = \frac{1}{3m(r)} \int_0^r g(r')K(r, r')\mathrm{d}r' \tag{9}$$

$$\frac{1}{\tau^{+}_{\text{coag}}(r)} = \frac{1}{3m(r)} \int_r^\infty g(r')K(r, r')\mathrm{d}r'. \tag{10}$$

Figure 10 shows τ_{coag}, τ^{+}_{coag}, and τ^{-}_{coag} for the base case for different points in time. As defined above, τ_{coag} represents the overall time scale due to coagulation, τ^{+}_{coag} is the time scale due to the uptake by larger droplets, τ^{-}_{coag} is the time scale due to the uptake by smaller droplets. All time scales show a characteristic minimum at $r_k = 42$ μm, which is the size of the droplets having the same response time as the Kolmogorov time scale τ_k for $\epsilon = 300$ cm^2 s^{-3}. Droplets of this size coagulate very fast so that they rush through this size range. The τ_{coag} curve is nonmonotonic and several regimes can be identified. At the start of the simulation, it increases up to $r = 15$ μm then decreases with a local minimum around $r = r_k$, followed by an increase again. A broadening effect results if the time scale decreases with increasing radius. At the beginning of the simulation period this condition is fulfilled for droplets with radius between 15 and 42 μm. Between these droplet sizes, τ_{coag} decreases over one magnitude. Later, this interval shrinks until after 30 min, the time scale is monotonically increasing. This means that a broadening effect due to coagulation is only expected at the early stage of cloud formation, which is however exactly the time when a mechanism is needed to enhance the formation of large droplets. Figure 10 also shows that once large droplets are formed, the τ_{coag} curve flattens, which means that all sizes grow with a similar speed. In Fig. 6, the size distributions after 40 min reflect this. The second mode with the large droplets shifts to the right without changing shape significantly.

Comparing τ^{+}_{coag} and τ^{-}_{coag} in Fig. 10 shows that the droplets of size r_k leave this size range because they are taken up by larger droplets—except for the first few minutes when the larger droplets are not yet formed.

Figure 11a displays τ_{coag} for different dissipation rates ($t = 5$ min.). The minimum of the time-scale shifts to smaller radii as the dissipation rate ϵ increases and the minimum value decreases from 30 min for $\epsilon = 50$ cm^2 s^{-3} to 1 s for $\epsilon = 500$ cm^2 s^{-3}. This relates to the time of the appearance of the second mode as well as to its position in Fig. 8. Larger dissipation rates decrease r_k and τ_{coag} causing the second mode to form earlier and closer to the first mode. On the other hand, for small ϵ, the size interval where a broadening effect can take place is larger. For $\epsilon = 50$ cm^2 s^{-3}, broadening occurs for the size range from 15 to 60 μm, whereas for $\epsilon = 500$ cm^2 s^{-3}, this interval is shortened and ranges from only 20 to 38 μm. Figure 11b shows that a variation of u' for a certain value of ϵ has a large effect on the absolute value of τ and affects the amplitude but not the position of the minimum with respect to the droplet size. Small values of u' favor the broadening effect.

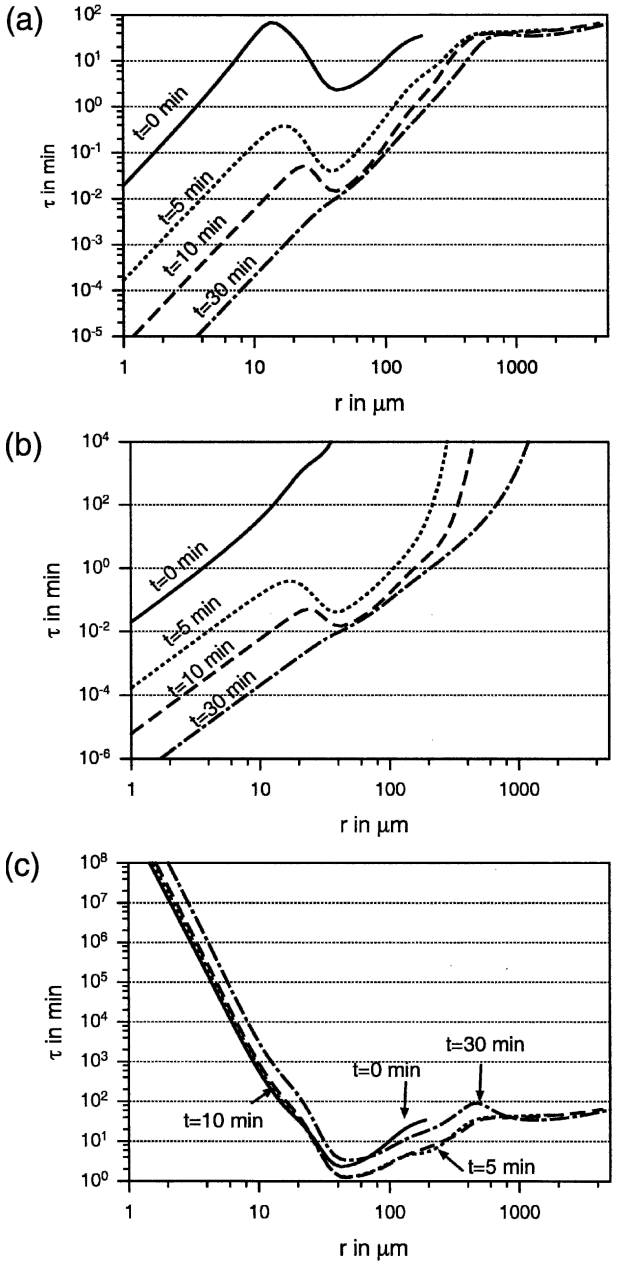

FIG. 10. Time scales (a) τ_{coag}, (b) τ^{+}_{coag}, and (c) τ^{-}_{coag} for the base case.

Coagulation and condensation occur simultaneously, so the broadening or narrowing effect by one process could therefore be enhanced or overcompensated by the other. To explore the relationships, Fig. 12 compares the time scales τ_{coag} and τ_{cond} at the start of simulation where we assume that coagulation and condensation are decoupled. The time scale τ_{cond} is calculated as described in section 3, so τ_{cond} has a singularity for the transport mean radius of the distribution because droplets of this size are assumed to be in equilibrium. Droplet sizes smaller than the transport mean evapo-

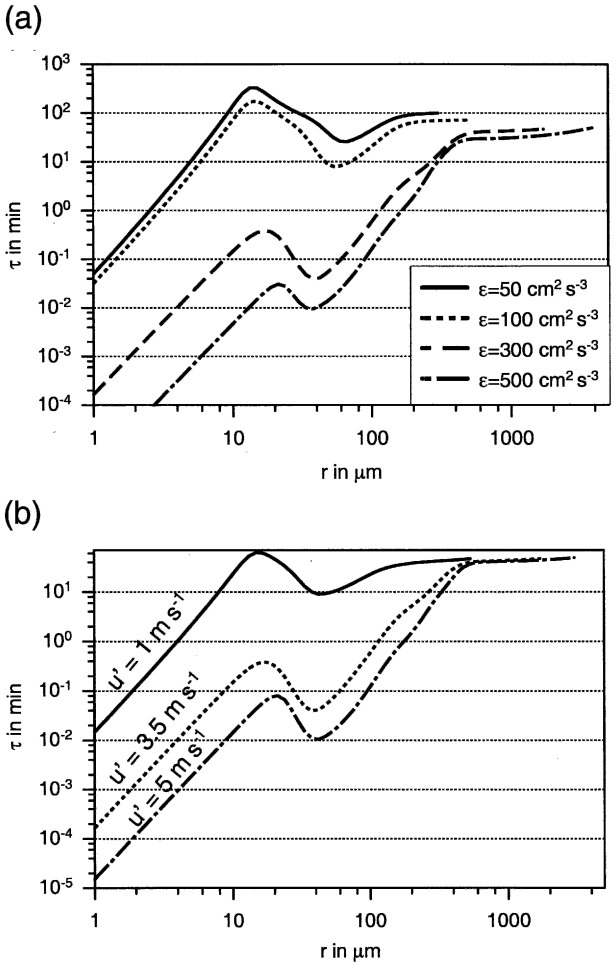

FIG. 11. (a) Time scales τ_{coag} for different dissipation rates. (b) Time scales τ_{coag} for $\epsilon = 300$ cm^2 s^{-3} and different u'.

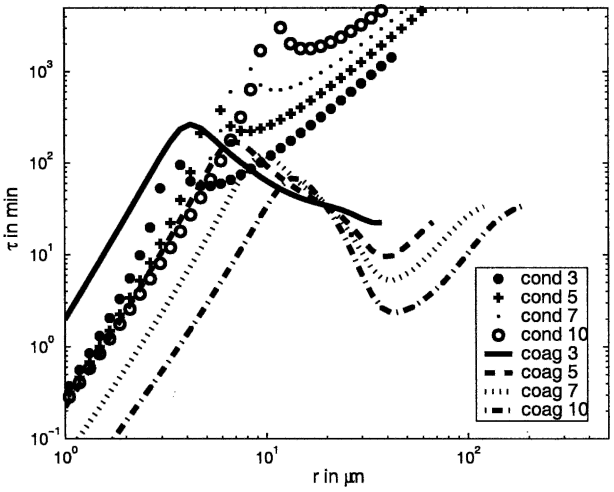

FIG. 12. Time scale τ_{coag} in comparison to τ_{cond} for different initial radii. The number in the legend denotes the respective initial radii in μm.

rate, while those larger than the transport mean grow. Figure 12 shows that for the case of a $r_{ini} = 3$ μm initial radius, τ_{cond} is by more than one magnitude smaller than τ_{coag} up to the radius of 10 μm. For the initial radius of 5 μm, τ_{coag} and τ_{cond} are on the same order of magnitude for the left tail of the distribution. For the initial radius of 7 and 10 μm, τ_{cond} exceeds τ_{coag} significantly.

Considering the size range smaller than the transport mean first, this behavior can be interpreted as follows: The small time scale τ_{cond} for the cases with small initial radii confirms the well-known finding that for very small droplets, condensation is the crucial process that alters the size distribution. By assuming that most of the droplets are in equilibrium with the ambient air, the small droplets are found to evaporate fast enough to broaden the size distribution to the left. This broadening occurs on a time scale shorter than τ_{coag}, which means that, overall, a broadening effect is expected toward the small sizes. For an initial radius of 5 μm, both processes have time scales of the same magnitude, which means that the droplets are removed from this size range by evaporation and by coagulation at a similar rate. From this examination alone it cannot be concluded what the overall effect will be since coagulation and condensation are not coupled in our model.

Considering the sizes larger than the transport mean, we find that, at first, for small initial radii narrowing because of condensation dominates but is overcome by broadening due to coagulation as the radii become larger.

4. Conclusions

In this paper we investigate the impact of turbulence on the development of cloud droplet spectra. To approach this problem, we solve the stochastic collection equation using a recently developed model by Zhou et al. (2001) to calculate the collision kernel for atmospheric conditions. The collision kernel accounts both for the transport and the accumulation effect.

The major uncertainties in this study are that the model by Zhou et al. (2001) was originally designed and validated for low Reynolds numbers and frozen turbulence. In our study we extrapolate their results to the atmosphere, an environment with extremely high Reynolds numbers and characterized by strong intermittency, without being able to confirm at this stage that this extrapolation holds. Furthermore, the kernel we use was developed for nonsedimenting particles. We approximate the presence of gravity by adding the turbulent and sedimentation kernels linearly, an approach which has to be confirmed or possibly refined once the interaction of turbulence and sedimentation is better understood. Keeping these limitations in mind we focus on two central questions, namely, if the rapid formation of large droplets can be reproduced and if we can ex-

plain the broadening of the size distribution toward both ends of the spectrum.

Compared to the effect of sedimentation in calm air only, we find that even moderate turbulence can enhance the formation of large droplets significantly. The largest impact of turbulence is expected for similar-sized particles and/or for particles in the size range smaller than 100 μm. Here, the collision kernel is enhanced by several orders of magnitude if turbulence is included, which accelerates the growth of droplets dramatically. While for calm air after 30-min simulation time, only 7% of the total mass is found in droplets with sizes over 100 μm, this is the case for 79% at a dissipation rate of 100 cm^2 s^{-3} and for 96% at 300 cm^2 s^{-3} if the combined sedimentation and turbulent kernel is considered. The accumulation effect in turbulence is the primary mechanism for this enhancement.

With a time-scale analysis we show that broadening toward the upper end of the spectrum is possible due to coagulation for about the first 15 min of the cloud development, depending on the turbulence intensity. Lower turbulence intensity implies a longer time interval for broadening.

A comparison of the time scale of coagulation with the time scale of condensation (for equilibrium conditions) shows that a trading of water between small droplets and large droplets due to the Kelvin effect can be responsible for the broadening toward the small end of the spectrum. This is especially effective if the mean radius of the size distribution is smaller than about 5 μm. If the mean radius is around 5 μm, the broadening due to evaporation for small droplets can be partially compensated by a narrowing due to coagulation. However, further studies with a model that includes the coupling between coagulation and condensation are necessary to judge the overall effect.

Thus it appears that the growth of droplets to drops is primarily due to the accumulation effect in turbulence when the droplet response times match the Kolmogorov time scale, and this also explains the broadening to larger drops on the right-hand side of the distributions. The broadening on the left can be explained by Kelvin effect–driven evaporation.

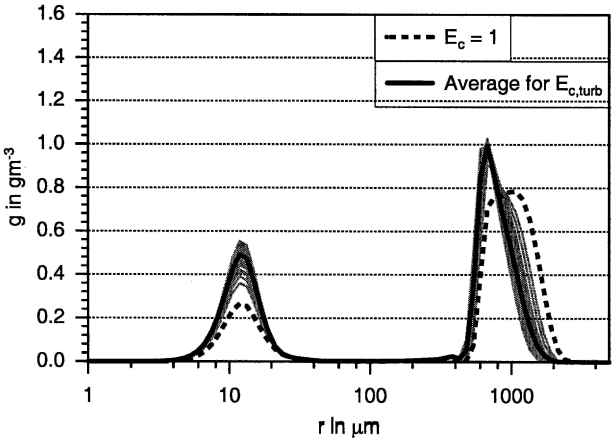

FIG. A1. Mass size distribution for $t = 30$ min, combined sedimentation and turbulent kernel, $\epsilon = 100$ cm^2 s^{-3}. Gray lines are results of 100 individual simulations with randomized collision efficiency (see text for details). Solid black line is average for randomized collision efficiency. Dotted black line is the case for $E_c = 1$.

APPENDIX

Turbulent Collision Efficiency

It is intuitively clear that the collision efficiency $E_{\text{col},t}$ must depend on the nature of the flow and particle size. The hydrodynamic interactions of droplets in turbulent flow are still an area of large uncertainties but there are indications that the collision efficiency is larger in a turbulent environment compared to calm air. Pinsky et al. (1999) have investigated this issue and conclude that the collision efficiency in a turbulent flow is a random value with a significant dispersion, the maximum value being several times larger than the mean value. To estimate the impact of the collision efficiency, the results of the study by Pinsky et al. (1999) are introduced in our study. Since they considered the case $\epsilon = 100$ cm^2 s^{-3} we will do the same and adopt their results for the averaged collision efficiency which is displayed in Fig. 14 of their paper. Results are available for three collector drop sizes (10, 20, and 30 μm). For collisions of droplets with both radii smaller than 30 μm, the values for the collision efficiency are two-dimensionally interpolated on our radius grid. Unfortunately, results are not available for larger sizes. However, the graphs in their Fig. 14 show that the collision efficiency approaches 1 as the collector droplets become larger. For the purposes of our estimation, we therefore use the value of 1 if one or both droplets are larger than 30 μm. To account for the randomness, we introduce for each time step random fluctuations around this averaged value of the collision efficiency in a way that the maximum deviation from the average is $\pm 70\%$.

With this modification, a set of 100 simulations is carried out. The results are shown for $t = 30$ min as gray lines in Fig. A1. Also, the average of these 100 simulations is shown and the result for the case $E_{\text{col},t} = 1$.

In all cases, the coagulation kernel consists of the sum of K_s and K_t ($\epsilon = 100$ cm^2 s^{-3} and $u' = 2.5$ m s^{-1}). Regarding the averaged result, the development of the large droplets is retarded compared to the case with $E_{\text{col},t} = 1$. However, a remarkable increase still has to be noted compared to the case of sedimentation in calm air only (Fig. 5). Given that, at higher dissipation rates, the values for $E_{\text{col},t}$ is expected to be even higher and considering the large uncertainties associated with the issue, it seems justified to retain the value $E_{\text{col},t} = 1$ throughout the study.

REFERENCES

Abrahamson, J., 1975: Collision rates of small particles in a vigorously turbulent fluid. *Chem. Eng. Sci.,* **30,** 1371–1379.

Arenberg, D., 1939: Turbulence as the major factor in the growth of cloud drops. *Bull. Amer. Meteor. Soc.,* **20,** 444–448.

Beard, K. V., and H. T. Ochs, 1993: Warm-rain initiation: An overview of microphysical mechanisms. *J. Appl. Meteor.,* **32,** 608–625.

Belin, F., J. Maurer, P. Tabeling, and H. Willaime, 1997: Velocity gradient distributions in fully developed turbulence: An experimental study. *Phys. Fluids,* **9,** 3843–3850.

Berry, E. X., 1967: Cloud droplet growth by collection. *J. Atmos. Sci.,* **24,** 688–700.

Bott, A., 1998: A flux method for the numerical solution of the stochastic collection equation. *J. Atmos. Sci.,* **55,** 2284–2293.

Brenguier, J.-L., and L. Chaumat, 2001: Droplet spectra broadening in cumulus clouds. Part I: Broadening in adiabatic cores. *J. Atmos. Sci.,* **58,** 628–641.

Butuirat, F., and M. Kielkiewicz, 1996: On additivity of coagulation kernels. *Ann. Nucl. Energy,* **23,** 1091–1096.

de Almeida, F. C., 1976: The collisional problem of cloud droplets moving in a turbulent environment—Part I: A method of solution. *J. Atmos. Sci.,* **33,** 1571–1578.

Friedlander, S. K., 1977: *Smoke, Dust, and Haze.* Wiley, 317 pp.

Grabowski, W. W., and P. Vaillancourt, 1999: Comments on "Preferential concentration of cloud droplets by turbulence: Effects of the early evolution of cumulus cloud droplet spectra." *J. Atmos. Sci.,* **56,** 1433–1436.

Grover, S. N., and H. R. Pruppacher, 1985: The effect of vertical turbulent fluctuations in the atmosphere on the collection of aerosol particles by cloud droplets. *J. Atmos. Sci.,* **42,** 2305–2318.

Hall, W. D., 1980: A detailed microphysical model within a two-dimensional dynamic framework: Model description and preliminary results. *J. Atmos. Sci.,* **37,** 2486–2507.

Jonas, P. R., and P. Goldsmith, 1972: The collection efficiencies of small droplets falling through a sheared air flow. *J. Fluid Mech.,* **52,** 593–608.

Kerminen, V.-M., and A. S. Wexler, 1995: Growth laws for atmospheric aerosol particles: An examination of the bimodality of the accumulation mode. *Atmos. Environ.,* **29,** 3262–3275.

Khain, A. P., and M. B. Pinsky, 1995: Drop inertia and its contribution to turbulent coalescence in convective clouds. Part I: Drop fall in the flow with random horizontal velocity. *J. Atmos. Sci.,* **52,** 196–206.

——, and ——, 1997: Turbulence effects on the collision kernel. II: Increase of the swept volume of colliding drops. *Quart. J. Roy. Meteor. Soc.,* **123,** 1543–1560.

——, M. Ovtchinnikov, M. Pinsky, A. Pokrovsky, and H. Krugliak, 2000: Notes of the state-of-the-art numerical modeling of cloud microphysics. *Atmos. Res.,* **55,** 159–224.

Kostinski, A. B., and R. A. Shaw, 2001: Scale-dependent droplet clustering in turbulent clouds. *J. Fluid Mech.,* **434,** 389–398.

Kruis, F. E., and K. A. Kusters, 1997: The collision rate of particles in turbulent flow. *Chem. Eng. Commun.,* **158,** 201–230.

Lee, I. Y., and H. R. Pruppacher, 1977: A comparative study on the growth of cloud drops by condensation using an air parcel model with and without entrainment. *Pure Appl. Geophys.,* **115,** 523–545.

MacPherson, J. I., and G. A. Isaac, 1977: Turbulent characteristics of some Canadian cumulus clouds. *J. Appl. Meteor.,* **16,** 81–90.

Majeed, M. A., and A. S. Wexler, 2001: Microphysics of aqueous droplets in clouds and fogs as applied to PM-fine modeling. *Atmos. Environ.,* **35,** 1639–1653.

Maxey, M. R., 1987: The gravitational settling of particles in homogeneous turbulence and random flow fields. *J. Fluid Mech.,* **174,** 441–465.

Neizvestny, A. I., and A. G. Kobzunenko, 1986: Effect of small-scale turbulence on the coagulation growth rate of cloud droplets. *Izv. Akad. Nauk SSSR, Fiz. Atmos. Okeana,* **22,** 626–633.

Park, S. H., F. E. Kruis, K. W. Lee, and H. Fissan, 2002: Evolution of particle size distributions due to turbulent and Brownian coagulation. *Aerosol Sci. Technol.,* **36,** 419–432.

Pinsky, M. B., and A. Khain, 1996: Simulations of drop fall in a homogeneous isotropic turbulent flow. *Atmos. Res.,* **40,** 223–259.

——, and ——, 1997a: Formation of inhomogeneity in drop concentration induced by the inertia of drops falling in a turbulent flow, and the influence of the inhomogeneity on the drop-spectrum broadening. *Quart. J. Roy. Meteor. Soc.,* **123,** 165–186.

——, and ——, 1997b: Turbulence effect on the collision kernel. I: Formation of velocity deviations of drops falling within a turbulent three-dimensional flow. *Quart. J. Roy. Meteor. Soc.,* **123,** 1517–1542.

——, and ——, 1997c: Turbulence effects on droplet growth and size distribution in clouds—A review. *J. Aerosol Sci.,* **28,** 1177–1214.

——, and ——, 2001: Fine structure of cloud droplet concentration as seen from the Fast-FSSP measurements. Part I: Method of analysis and preliminary results. *J. Appl. Meteor.,* **40,** 1515–1537.

——, ——, and M. Shapiro, 1999: Collisions of small drops in a turbulent flow. Part I: Collision efficiency. Problem formulation and preliminary results. *J. Atmos. Sci.,* **56,** 2585–2600.

——, ——, and ——, 2000: Stochastic effects of cloud droplet hydrodynamic interaction in a turbulent flow. *Atmos. Res.,* **53,** 131–169.

Pruppacher, H. R., and J. D. Klett, 1997. *Microphysics of Clouds and Precipitation.* 2d ed. Kluwer Academic, 954 pp.

Reade, W. C., and L. R. Collins, 2000: Effect of preferential concentration on turbulent collision rates. *Phys. Fluids,* **12,** 2530–2540.

Rogers, R. R., and M. K. Yau, 1989. *A Short Course in Cloud Physics.* 3d ed. Butterworth-Heinemann, 290 pp.

Saffman, P. G., and J. S. Turner, 1956: On the collision of drops in turbulent clouds. *J. Fluid Mech.,* **1,** 16–30.

Shaw, R. A., 2000: Supersaturation intermittency in turbulent clouds. *J. Atmos. Sci.,* **57,** 3452–3456.

——, 2003: Particle–turbulence interactions in atmospheric clouds. *Annu. Rev. Fluid Mech.,* **35,** 183–227.

Squires, K. D., and J. K. Eaton, 1991: Preferential concentration of particles by turbulence. *Phys. Fluids,* **A3,** 1169–1179.

Sundaram, S., and L. R. Collins, 1996: Numerical considerations in simulating a turbulent suspension of finite-volume particles. *J. Comput. Phys.,* **124,** 337–350.

——, and ——, 1997: Collision statistics in an isotropic, particle-laden turbulent suspension. I. Direct numerical simulations. *J. Fluid Mech.,* **335,** 75–110.

Vaillancourt, P. A., and M. K. Yau, 2000: Review of particle–turbulence interactions and consequences for cloud physics. *Bull. Amer. Meteor. Soc.,* **81,** 285–298.

——, ——, P. Bartello, and W. W. Grabowski, 2002: Microscopic approach to cloud droplet growth by condensation. Part II: Turbulence, clustering and condensational growth. *J. Atmos. Sci.,* **59,** 3421–3435.

Vohl, O., S. K. Mitra, S. C. Wurzler, and H. R. Pruppacher, 1999: A wind tunnel study of the effects of turbulence on the growth of cloud drops by collision and coalescence. *J. Atmos. Sci.,* **56,** 4088–4099.

Wang, L.-P., and M. R. Maxey, 1993: Settling velocity and con-

centration distribution of heavy particles in homogeneous isotropic turbulence. *J. Fluid Mech.,* **335,** 27–68.
——, A. S. Wexler, and Y. Zhou, 1998: Statistical mechanical description of turbulent coagulation. *Phys. Fluids,* **10,** 2647–2651.
——, ——, and ——, 2000: Statistical mechanical description and modelling of turbulent collision of inertial particles. *J. Fluid Mech.,* **415,** 117–153.
Warner, J., 1969: The microstructure of cumulus cloud. Part I. General features of the droplet spectrum. *J. Atmos. Sci.,* **26,** 1049–1065.
Williams, J. J. E., and R. I. Crane, 1983: Particle collision rate in turbulent flow. *Int. J. Multiphase Flow,* **9,** 421–435.
Woods, J. D., P. Goldsmith, and J. C. Drake, 1972: Coalescence in a turbulent cloud. *Quart. J. Roy. Meteor. Soc.,* **98,** 135–149.
Yin, Y., Z. Levin, T. Reisin, and S. Tzivion, 2000: The effects of giant cloud condensation nuclei on the development of precipitation in convective clouds: A numerical study. *Atmos. Res.,* **53,** 91–116.
Zhou, Y., A. S. Wexler, and L.-P. Wang, 2001: Modelling turbulent collision of bidisperse inertial particles. *J. Fluid Mech.,* **433,** 77–104.